Restle, Tassilo M. F.; Zeitz, Sabine; Meyer, Jan; Klein, Wilhelm; Raudaschl-Sieber, Gabriele; Karttunen, Antti J.; Fässler, Thomas F.

Aliovalent substitution in phosphide-based materials – Crystal structures of $Na_{10}AlTaP_6$ and Na_3GaP_2 featuring edge-sharing EP_4 tetrahedra (E=Al/Ta and Ga)

Published in:
Zeitschrift fur Anorganische und Allgemeine Chemie

DOI:
10.1002/zaac.202100149

Published: 27/09/2021

Document Version
Publisher's PDF, also known as Version of record

Journal of Inorganic and General Chemistry
ZAAC
Zeitschrift für anorganische und allgemeine Chemie
DOI: 10.1002/zaac.202100149
ARTICLE

Aliovalent substitution in phosphide-based materials – Crystal structures of $Na_{10}AlTaP_6$ and Na_3GaP_2 featuring edge-sharing EP_4 tetrahedra (E = Al/Ta and Ga)

Tassilo M. F. Restle,[a] Sabine Zeitz,[a] Jan Meyer,[a] Wilhelm Klein,[a] Gabriele Raudaschl-Sieber,[b] Antti J. Karttunen,[c] and Thomas F. Fässler*[a]

Dedicated to Professor Hansgeorg Schnöckel on the Occasion of His 80th Birthday.

Recently, ternary lithium phosphides have been studied intensively owing to their high lithium ion conductivities. Much less is known about the corresponding sodium-containing compounds, and during investigations aiming for sodium phosphidotrielates, two new compounds have been obtained. The sodium phosphidoaluminumtantalate $Na_{10}AlTaP_6$, at first obtained as a by-product from the reaction with the container material, crystallizes in the monoclinic space group $P2_1/n$ (no. 14) with lattice parameters of a = 8.0790(3) Å, b = 7.3489(2) Å, c = 13.2054(4) Å, and β = 90.773(2)°. The crystal structure contains dimers of edge-sharing $[(Al_{0.5}Ta_{0.5})P_4]$ tetrahedra with a mixed Al/Ta site. DFT calculations support the presence of this type of arrangement instead of homonuclear Al_2P_6 or Ta_2P_6 dimers. The ^{31}P and ^{23}Na MAS NMR as well as the Raman spectra confirm the structure model. The assignment of the chemical shifts is confirmed applying the DFT-PBE method on the basis of the ordered structural model with mixed $AlTaP_6$ dimers. The sodium phosphidogallate Na_3GaP_2 crystallizes in the orthorhombic space group *Ibam* (no. 72) with lattice parameters of a = 13.081(3) Å, b = 6.728(1) Å, and c = 6.211(1) Å and is isotypic to Na_3AlP_2. Na_3GaP_2 exhibits linear chains of edge-sharing $^1_\infty[GaP_{4/2}]$ tetrahedra. For both compounds band structure calculations predict indirect band gaps of 2.9 eV.

Introduction

During the last years, lithium phosphide-based materials have been discovered as promising candidates for solid electrolytes due to a very good ionic conducting behavior of some representatives. The structural building units in these phosphides are basically EP_4 tetrahedra (E = a tetrel or triel element), which are surrounded by lithium atoms. Isolated $[TtP_4]^{8-}$ and $[TrP_4]^{9-}$ tetrahedra (Tt = Si, Ge, Sn; Tr = Al, Ga) were found in compounds with the highest Li contents, Li_8TtP_4, Li_9TrP_4 and $Li_{14}TtP_6$.[1–5] The highest lithium ionic conductivity of 3×10^{-3} S cm^{-1} has been observed for the lithium phosphidoaluminate Li_9AlP_4.[4] The dependence of the conductivity from the amount of positive charge carriers necessary to compensate the negative charge of the tetrahedral anions is obvious and still subject of investigations. The idea behind phosphide-based materials as ionic conductors originates from the aliovalent substitution of $[TtS_4]^{4-}$ tetrahedra (Tt = tetrel element), which are the main building blocks in the well-examined sulfide-based conductors. The so obtained analogous $[TtP_4]^{8-}$ units then allow the accommodation of more cations for charge compensation of the eight-fold negative charge of the tetrahedra.

By reducing the amount of lithium in phosphidotetrelates many different structures with condensed and covalently connected tetrahedra are observed. Illustrative examples of this manifold structural variety are $Li_{10}Si_2P_6$, which features edge-sharing SiP_4 double tetrahedra,[6] Li_2SiP_2/Li_2GeP_2 and $LiSi_2P_3$,[7–9] where SiP_4 and GeP_4 tetrahedra are condensed to a network of super-tetrahedra, $Li_3Si_3P_7$ with double layers formed by vertex-sharing SiP_4 tetrahedra,[6] and $LiGe_3P_3$ with a two-dimensional polyanion comprising GeP_4 and Ge(P_3Ge) tetrahedra.[8]

A formally aliovalent substitution of the tetrel by a triel element leads to the lithium phosphidotrielates Li_3AlP_2 and Li_3GaP_2 which contain two-dimensional layers of corner- and edge-sharing tetrahedra,[4,10] whereas the corresponding Li_3InP_2 shows a polyanionic framework of corner-sharing InP_4 super-tetrahedra.[11]

[a] T. M. F. Restle, S. Zeitz, J. Meyer, W. Klein, T. F. Fässler
Department of Chemistry,
Chair of Inorganic Chemistry with Focus on New Materials,
Technische Universität München,
Lichtenbergstraße 4, D-85747 Garching,
Germany
E-mail: Thomas.Faessler@lrz.tum.de
[b] G. Raudaschl-Sieber
Department of Chemistry,
Chair of Inorganic and Metal-Organic Chemistry,
Technische Universität München,
Lichtenbergstraße 4, D-85747 Garching,
Germany
[c] A. J. Karttunen
Department of Chemistry and Materials Science,
Aalto University, FI-00076, Espoo,
Finland

Supporting information for this article is available on the WWW under https://doi.org/10.1002/zaac.202100149

While lithium-based phosphides have already been studied intensively, much less is reported about the corresponding sodium species. $Na_{10}Si_2P_6$ and $Na_{10}Ge_2P_6$ contain dimers of SiP_4 and GeP_4 tetrahedra, respectively,[12] Na_2SiP_2 comprises infinite chains of edge-sharing tetrahedra,[13] 2D and 1D polyanions are present in $NaGe_3P_3$ and $Na_{4+n}Ge_{6+n}P_{6-n}$ ($n=0$, 1), respectively,[14–15] and the series $Na_{23}Si_{9n+19}P_{12n+33}$ ($n=0$–3), $Na_{19}Si_{13}P_{25}$, *LT*-$NaSi_2P_3$ and *HT*-$NaSi_2P_3$ are built up by 3D-connected SiP_4 super-tetrahedra.[16]

Even less is known about sodiumphosphidotrielates, and only one sodium phosphidoaluminate (Na_3AlP_2), one sodium phosphidogallate (Na_6GaP_3) and one sodium phosphidoindate (Na_3InP_2) have been reported.[17–19] The sodium phosphidogallate Na_6GaP_3 contains trigonal-planar GaP_3 triangles,[19] and although Na_3AlP_2 and Na_3InP_2 have similar compositions, they are not isotypic and exhibit different connectivity patterns of the $M^{III}P_4$ tetrahedra. In the former, edge-sharing AlP_4 tetrahedra are forming one-dimensional chains,[17] whereas InP_4 units build a three-dimensional polyanionic framework of corner- and edge-sharing tetrahedra in the latter.[18]

Here we report the synthesis and characterization of two new compounds, the first sodium aluminum–tantalum phosphide $Na_{10}AlTaP_6$ and the ternary compound Na_3GaP_2, both exhibiting edge-sharing MP_4 tetrahedra.

Experimental Section

All steps of synthesis and sample preparations were carried out inside an argon-filled glove box (*MBraun*, $p(H_2O)$, $p(O_2) < 0.1$ ppm). Prior to use, sodium (Na, rods, Merck-Schuchardt, >99%) was cleaned from oxide layers. Aluminum (Al, granules, ChemPur, 99.99%), gallium (Ga, pellets, Alfa Aesar, 99.99999%), tantalum (Ta, powder, Alfa Aesar, 99.98%) and phosphorus (P, powder, Sigma-Aldrich, 97%) were used as obtained without further purification.

Synthesis of $Na_{10}AlTaP_6$. Single crystals of $Na_{10}AlTaP_6$ were obtained as red blocks by the reaction of sodium, aluminum and phosphorus with the nominal composition "$Na_3Al_3P_4$" in a tantalum tube. Sodium (130.0 mg, 5.59 mmol, 3.0 equiv.), aluminum (151.0 mg, 5.60 mmol, 3.0 equiv.) and phosphorus (238.3 mg, 7.46 mmol, 4.0 equiv.) were filled into a tantalum tube. The tube was sealed in an electric arc furnace, enclosed in a silica reaction container under vacuum and subsequently heated with 5 $K \cdot min^{-1}$ to 1073 K, dwelled for 24 h, and cooled with 0.5 $K \cdot min^{-1}$ to room temperature in a tube furnace, yielding a dark-grey product with red-shining crystals of $Na_{10}AlTaP_6$.

Bulk samples of $Na_{10}AlTaP_6$ were synthesized from the elements via ball-milling and subsequent annealing. Sodium (1082.0 mg, 30.4 mmol, 10 equiv.), aluminum (127.0 mg, 4.7 mmol, 1 equiv.), tantalum (851.6 mg, 4.7 mmol, 1 equiv.), and phosphorus (874.6 mg, 17.1 mmol, 6 equiv.) were ball-milled (Retsch PM100 Planetary Ball Mill) for 36 h at 350 rpm with rest periods (every 10 min for 3 min) using a WC milling set (50 mL jar, 3 balls with a diameter of 1.5 cm). The obtained black powder was pressed into pellets with a diameter of 13 mm for 30 s at 5 t using a hydraulic press (Specac Atlas 15T). The fragmented pellets were filled into a niobium tube (8 mm diameter), which was sealed in an electric arc furnace (Edmund Bühler MAM1), enclosed in a silica reaction container under vacuum, heated with 5 $K \cdot min^{-1}$ to 973 K, dwelled for 36 h, and cooled with 0.5 $K \cdot min^{-1}$ to room temperature in a tube furnace (HTM Reetz Loba 1200-42-600-1-OW with a EUROTHERM S 14083 temperature controller). After grinding of the pellets, a dark red-brown powder was obtained. Besides $Na_{10}AlTaP_6$, the sample showed reflections of Na_7TaP_4 with very low intensity.

Synthesis of Na_3GaP_2. Single crystals of Na_3GaP_2 were obtained as red plates by the reaction of sodium, gallium and phosphorus with nominal composition "Na_9GaP_4" in a tantalum tube. Sodium (198.2 mg, 8.54 mmol, 9.0 equiv.), gallium (66.1 mg, 0.95 mmol, 1.0 equiv.) and phosphorus (121.1 mg, 3.79 mmol, 4.0 equiv.) were filled into a tantalum tube. The tube was sealed in an electric arc furnace, enclosed in a silica reaction container under vacuum, subsequently heated with 5 $K \cdot min^{-1}$ to 1073 K, dwelled for 24 h, and cooled with 0.5 $K \cdot min^{-1}$ to room temperature in a tube furnace, yielding a grey-brown product with red-shining crystals of Na_3GaP_2. The best attempts to synthesize single-phase Na_3GaP_2 was achieved by ball-milling of the elements in stoichiometric ratio and subsequently annealing at 1023 K with cooling rapidly to room temperature yielding Na_3GaP_2 as the main product accompanied with at least one unknown phase (see Figure S7).

Powder X-ray diffraction. For powder X-ray diffraction (PXRD) measurements, the samples were ground in an agate mortar and sealed inside 0.3 mm glass capillaries. PXRD measurements were performed at room temperature on a Stadi P diffractometer (Stoe & Cie) equipped with a MYTHEN DCS 1 K (Dectris) solid-state detector, a Ge(111) monochromator for Mo $K_{\alpha1}$ radiation ($\lambda = 0.7093$ Å) for the ball mill-synthesized $Na_{10}AlTaP_6$, and Cu $K_{\alpha1}$ radiation ($\lambda = 1.5406$ Å) for the products from the syntheses of "$Na_3Al_3P_4$" and "Na_9GaP_4". The raw powder data were processed with the software package WinXPOW.[20]

Rietveld refinement. The Rietveld refinement of $Na_{10}AlTaP_6$ was carried out with TOPAS V6.[21] The single crystal structure data were used as the starting model. In the last refinement cycles, the unit cell parameters, atom positions, isotropic displacement parameters, and the site occupancy factor of Al/Ta were refined. Al and Ta were restrained to identical positional and displacement parameters, and one joint displacement parameter was assigned for all five independent Na and one for all three independent P atom positions.

Single crystal structure determination. Single crystals of $Na_{10}AlTaP_6$ and Na_3GaP_2 were sealed in 0.3 mm glass capillaries. The single crystal X-ray diffraction (SCXRD) measurements were performed on a Stadivari diffractometer (Stoe & Cie) equipped with a Ge(111) monochromator, an Mo K_α radiation ($\lambda = 0.71073$ Å) source and a PILATUS 3R 300 K detector (Dectris). The structures were solved by Direct Methods (SHELXS) and refined by full-matrix least-squares calculations against F^2 (SHELXL).[22] In case of $Na_{10}AlTaP_6$, Ta and Al are found to share one crystallographic site, and the occupation factor was refined to almost exactly 50% for each element. The positional and displacement parameters have been restrained to identical values for both elements. Further details of the crystal structure investigations may be obtained from the joint CCDC/FIZ Karlsruhe online deposition service: https://www.ccdc.cam.ac.uk/structures/? by quoting the depository numbers CSD-2072301 ($Na_{10}AlTaP_6$) and CSD-2072302 (Na_3GaP_2).

Impedance spectroscopy. The electrochemical impedance spectroscopy for $Na_{10}AlTaP_6$ was performed in an in-house designed cell. The detailed setup and procedure are described by Restle *et al.*.[4] Powdered samples of $Na_{10}AlTaP_6$ (200 mg) were placed between two 8 mm dies, and the screws were tightened with a torque of 30 Nm, thereby compressing the samples to 85% of the theoretical density. Impedance spectra were recorded on a Bio-Logic potentiostat (SP-300) in a frequency range from 7 MHz to 50 mHz at a potentiostatic excitation of ±10 mV. Data were treated using the software EC-Lab (V 11.27). The measurements were performed in an

Ar-filled glove box at 298 K. The electronic conductivity was determined with the same setup using a potentiostatic polarization procedure and voltages of 50, 100 and 150 mV for 7 h each.

NMR Spectroscopy. Magic angle spinning (MAS) NMR spectra of $Na_{10}AlTaP_6$ were recorded on a Bruker Avance 300 NMR device operating at 7.04 T in a 4 mm ZrO_2 rotor. The resonance frequencies of the nuclei were 79.39 and 121.46 MHz for ^{23}Na and ^{31}P, respectively. The rotational frequency was set to 13 and 15 kHz for ^{31}P and 15 kHz for ^{23}Na. The MAS spectra were obtained at room temperature with relaxation delays of 10 s (^{23}Na) and 30 s (^{31}P), and 1080 (^{23}Na) and 1688 scans (^{31}P). The ^{23}Na spectrum is referenced to NaCl (1 M, aq.) and NaCl (s) with chemical shifts of 0.00 and +7.20 ppm, respectively. The ^{31}P spectrum is referred to ammonium dihydrogen phosphate (s) with a chemical shift of 1.11 ppm with reference to concentrated H_3PO_4. All spectra were recorded using single-pulse excitation.

Raman Spectroscopy. A Raman spectrum of the bulk material of $Na_{10}AlTaP_6$ was measured using an inVia Raman microscope (Renishaw, RE04), equipped with a CCD detector. The powdered sample was sealed into a 0.5 mm glass capillary and irradiated with a 785 nm laser beam for 1 s at 0.5 % laser power using a microscope equipped with a 50-fold magnifying objective and a grating with 1800 lines mm^{-1}. For the final spectrum 100 single measurements were averaged. The software WiRe 4.2 (build 5037, Renishaw 2002) was used for data recording.[23]

Electronic Structure Calculations. The structure and the electronic and vibrational properties of $Na_{10}AlTaP_6$ and Na_3GaP_2 were studied using the CRYSTAL17 program package and hybrid density functional methods.[24] A hybrid exchange correlation functional after Perdew, Burke and Ernzerhof (DFT-PBE0),[25–26] and Localized Gaussian-type triple-zeta valence+polarization level basis sets derived from the Karlsruhe basis sets were applied (split-valence+polarization level basis set for Na, all basis sets are listed in the Supporting Information).[27–28] For the evaluation of the Coulomb and exchange integrals (TOLINTEG), tight tolerance factors of 8, 8, 8, 8, 16 were used for all calculations. The reciprocal space of $Na_{10}AlTaP_6$ and Na_3GaP_2 was sampled with 4×5×2 and 4×4×4 Monkhorst-Pack-type *k*-point grids, respectively.[29] The starting geometries were taken from the experimental data, and the lattice parameters and atomic positions were fully optimized within the constraints imposed by the space group symmetry. For calculations of $Na_{10}AlTaP_6$, the symmetry of the experimental structure was reduced to *P*1*c*1 where the Ta/Al 4*e* mixed position is split into a 2*a* position for Ta and Al each. The optimized structures were confirmed to be true local minima by means of harmonic frequency calculations at the Γ-point.[30–31] Raman intensities were obtained with the Coupled Perturbed Kohn-Sham method implemented in CRYSTAL.[32–33] For $Na_{10}AlTaP_6$, the theoretical Raman spectrum was calculated at room temperature with an excitation wavelength of 785 nm. Raman spectra were broadened using pseudo-Voigt peak profile (50:50 Lorenzian:Gaussian) and FWHM of 8 cm^{-1}. The vibrational spectra were interpreted by visual inspection of the normal modes using the Jmol program.[34] The reciprocal space coordinates for the electronic band structure plots were obtained from the SeeK-path web service;[35–36] the used band paths are listed in the Supporting Information.

The solid-state NMR magnetic shielding tensors (^{31}P and ^{23}Na) of $Na_{10}AlTaP_6$ were calculated with the DFT-PBE method[25] using the CASTEP program package and the GIPAW formalism as implemented in CASTEP-NMR.[37–39] Ultrasoft pseudopotentials generated with the on-the-fly scheme and a plane-wave basis set cut-off of 660 eV were applied.[40] The reciprocal space was sampled using a 2×2×1 Monkhorst-Pack-type *k*-mesh. The NMR shielding tensors were obtained at the experimental geometry within the *P*1*c*1 structural model described above. Solid $(NH_4)H_2PO_4$ and NaCl were used as references to convert the computed shieldings to ^{31}P and ^{23}Na chemical shifts. Their structures were fully optimized with a total energy convergence criterion of 0.5×10^{-6} eV/atom. 3×3×3 and 8×8×8 *k*-meshs were used for $(NH_4)H_2PO_4$ (*I*-42*d*) and NaCl (*Fm*-3*m*), respectively. The isotropic shieldings of the reference species are 280.16 ppm for ^{31}P and 544.91 ppm for ^{23}Na.

Results and Discussion

Synthesis and crystal structure of $Na_{10}AlTaP_6$. Similar to the first results obtained for Na_7TaP_4[41] the title compound was received in an explorative synthesis of sodium phosphidoaluminates in a tantalum tube. Almost pure $Na_{10}AlTaP_6$ was synthesized from the elements via a two-step procedure. At first, stoichiometric amounts of the elements Na, Al, Ta, and P were ball-milled resulting in a reactive mixture which according to the powder X-ray diffractogram contained mainly tantalum (see Figure S4). Subsequently, the powder mixture was annealed at 973 K for 36 hours, yielding $Na_{10}AlTaP_6$ accompanied by small amounts of Na_7TaP_4 (see Figure 1). Powdered $Na_{10}AlTaP_6$ is red-brown. Complete data of the Rietveld refinement are given in the Supporting Information (Tables S4 and S5). The $Na_{10}AlTaP_6$:Na_7TaP_4 ratio is 97.3(2) wt.-%:2.7(2) wt.-% as determined by Rietveld refinement.

Red single crystals of $Na_{10}AlTaP_6$ were obtained from the reaction of the elements in the ratio Na:Al:P = 3:3:4 at 1073 K in a tantalum tube. Besides $Na_{10}AlTaP_6$, the resulting mixture contains AlP, TaP and Na_3AlP_2 (see Figure S5). Details of the structure refinement of the single crystal X-ray diffraction of $Na_{10}AlTaP_6$ are listed in Table 1 (further data are given in Tables S1 and S2 in the Supporting Information).

$Na_{10}AlTaP_6$ crystallizes in the monoclinic space group $P2_1/n$ (no. 14), with all nine crystallographically independent atoms at general 4*e* positions (five Na and three P, Al/Ta at one mixed position). The mixed aluminum/tantalum position is refined to 50 % within a 3σ error range. The crystal structure of $Na_{10}AlTaP_6$ is shown in Figure 2 with displacement ellipsoids set at 90 % probability at 150 K. The structure is built up by dimers of edge-sharing $[(Al_{0.5}Ta_{0.5})P_4]$ tetrahedra which are separated by Na atoms. $Na_{10}AlTaP_6$ is charge-balanced according to the oxidation states Na^+, Al^{3+}, Ta^{5+}, and P^{3-}, and by taking into account covalent Ta–P and Al–P bonds; it can be written as $(Na^+)_{10}[AlTaP_6]^{10-}$.

The crystal structure can be described as a distorted hexagonal close packing of phosphorus atoms with 24 tetrahedral and 12 octahedral voids per unit cell according to the multiplicity of the phosphorous' Wyckoff positions (3×4*e*). The distorted *hcp* of P atoms is emphasized in Figure 2c by an *ABAB* layer sequence of P atoms in direction of the *b* axis, resulting in distorted NaP_6 octahedra which are sharing faces perpendicular to *b*. One sixth of the tetrahedral voids are statistically filled by equal amounts of aluminum and tantalum atoms. The sodium atoms occupy all octahedral (Na1, Na2 and Na5) and eight of the remaining tetrahedral voids (Na3 and Na4). Hence, the

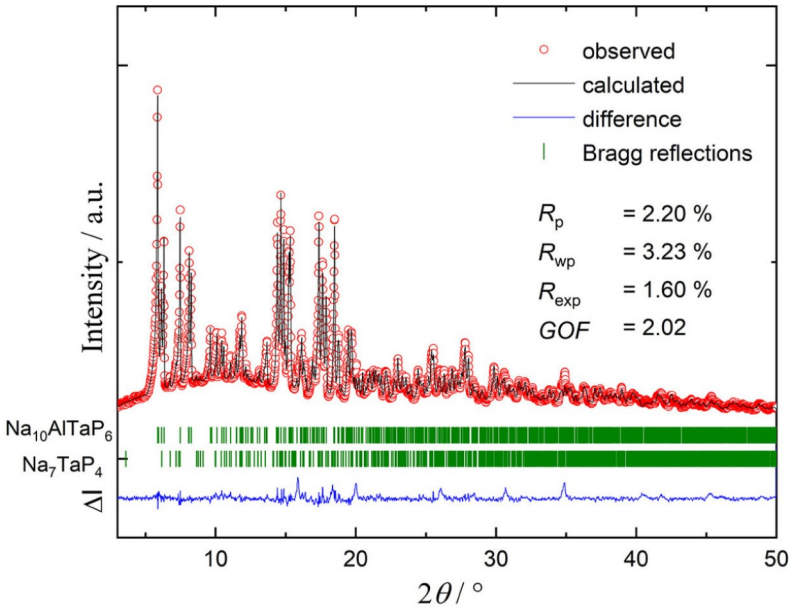

Figure 1. Rietveld analysis of the powder X-ray diffractogram of $Na_{10}AlTaP_6$. The red line indicates the observed intensities, the black line shows the calculated intensities, and the blue line corresponds to the difference between both. Bragg positions are marked by green dashes. The $Na_{10}AlTaP_6$:Na_7TaP_4 ratio is 97.3(2) wt.-%:2.7(2) wt.-%.

Table 1. Crystallographic Data and refinement parameters of the SCXRD analysis of $Na_{10}AlTaP_6$ and Na_3GaP_2.

Empirical formula	$Na_{10}Al_{0.998(1)}Ta_{1.002(1)}P_6$	Na_3GaP_2
Formula weight/g·mol^{-1}	623.64	200.64
Crystal size/mm^3	0.25×0.2×0.15	0.1×0.1×0.02
Crystal color	red	red
Crystal shape	block	plate
T/K	150	150
Space group	$P2_1/n$ (no. 14)	*Ibam* (no. 72)
Unit cell dimension/Å	*a* = 8.0790(3)	*a* = 13.0808(14)
	b = 7.3489(2)	*b* = 6.7278(6)
	c = 13.2054(4)	*c* = 6.2109(6)
	β = 90.773(2)°	
V/Å^3	783.96(4)	546.59(9)
Z	2	4
ρ (calc.)/g·cm^{-3}	2.642	2.438
μ/mm^{-1}	7.921	5.685
2*θ* Range/deg	2.9–57.5	2.9–57.5
Index range *hkl*	−17 < h < 17	−23 < h < 23
	−12 < k < 15	−12 < k < 10
	−28 < l < 28	−11 < l < 10
Reflections collected	101159	11624
Independent reflections	8231	913
R_{int}	0.025	0.028
Reflections with $I > 2\sigma(I)$	7626	804
Data/restraints/parameter	8231/0/84	913/0/20
Absorption correction	empirical	empirical
Goodness-of-fit on F^2	1.124	1.066
Final *R* indices $[I > 2\sigma(I)]^{a,b}$	R_1 = 0.0197	R_1 = 0.0183
	wR_2 = 0.0436	wR_2 = 0.0385
R indices (all data) ^{a,b}	R_1 = 0.0227	R_1 = 0.0236
	wR_2 = 0.0444	wR_2 = 0.0403
Largest diff. peak and hole/e Å^{-3}	2.50/−1.91	0.62/−0.78
Depository numbers	CSD-2072301	CSD 2072302

octahedral voids are fully occupied, whereas the tetrahedral voids are filled to 50%.

The formation of dimers of MP_4 tetrahedra comprising 50% Al and 50% Ta results in the possibility to form either mixed dimers Al_2P_6 or a superposition of the dimers Al_2P_6 and Ta_2P_6 with equal contribution. Certainly a superposition of all three dimers is possible as well. DFT-PBE0 calculations on an ordered structural model consisting of mixed $AlTaP_6$ dimers (space group *P*1*c*1) show that this model is 144 kJ/mol per unit cell lower in energy compared to an ordered structural model with Al_2P_6 and Ta_2P_6 dimers (space group *P*-1). Thus, from an energetic point of view, the mixed dimers are clearly favored over the uniform ones.

The $(Al_{0.5}Ta_{0.5})P_4$ tetrahedra in $Na_{10}AlTaP_6$ are slightly distorted with a narrow P3–(Ta/Al)–P3 angle of 101.468(7)° due to the repulsion between the highly charged central atoms; the remaining angles range from 108.037(8)° to 114.167(8)° and are closer to the ideal tetrahedron angle. The (Al/Ta)–P bond lengths range from 2.4055(2) to 2.4410(2) Å and are between Ta–P distances in compounds with isolated TaP_4 tetrahedra like Na_7TaP_4,[41] Na_5SrTaP_4 (2.3856–2.4108 Å),[42] $Na_{5.15}Eu_{0.85}TaP_4$ (2.378(5)–2.399(2) Å)[43] or K_5BaTaP_4 (2.3980(1)–2.4115(1) Å),[44] and Al–P distances in compounds with isolated AlP_4 tetrahedra like Li_9AlP_4 (2.425(1) and 2.433(1) Å).[4] These very similar *M*–P distances resp. ionic radii might be the main reason for the Al/Ta disorder as they are too similar to induce a site separation within one anion. All sodium atoms exhibit strongly distorted coordination polyhedra, as shown in Figure S1. The distortion of the NaP_4 tetrahedra (Na3 and Na4) is mirrored in the P–Na–P angles ranging from 88.681(1)° to 119.625(1)°; the Na–P distances are between 2.8558(1) and 3.0413(1) Å and thus very

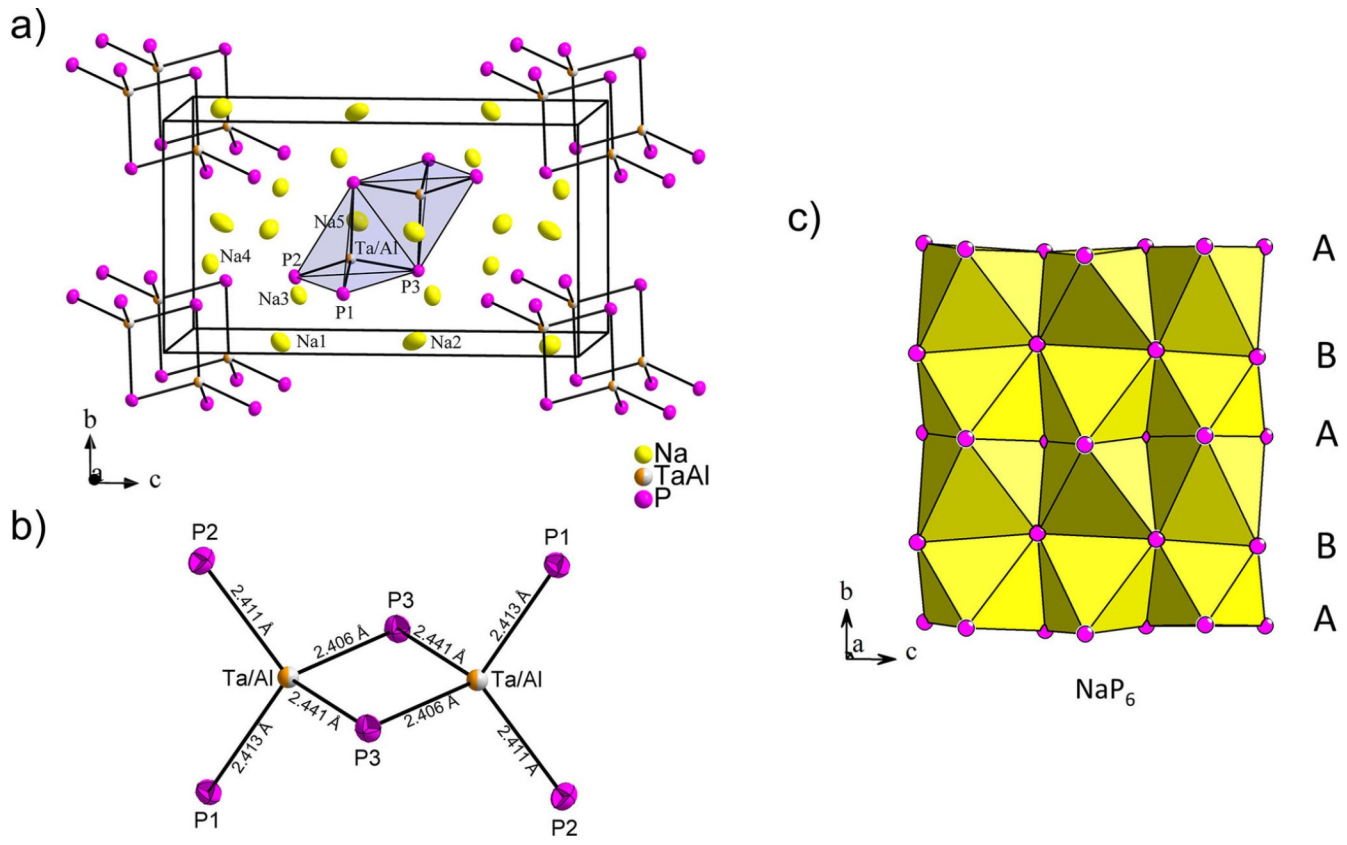

Figure 2. The crystal structure of $Na_{10}AlTaP_6$. a) Extended unit cell with edge-sharing $[Al_{0.5}Ta_{0.5}P_4]$ tetrahedra. b) Dimeric $AlTaP_6$ tetrahedra with bond distances. c) ABAB layers of face-sharing NaP_6 octahedra, illustrating the *hcp* of the phosphorous atoms. The Na, Al, Ta, and P atoms are drawn in yellow, orange, grey, and purple, respectively. The displacement ellipsoids are shown at a 90 % probability level.

similar to those in Na_3P.[45] The distortion of the NaP_6 octahedra (Na1, Na2 and Na5) is illustrated by a huge range of Na–P distances between 2.8758(1) and 4.3949(1) Å, also indicating that the Na atoms are not located in the center of gravity of the respective P_6 octahedron.

$Na_{10}AlTaP_6$ is isotypic to $Na_{10}Si_2P_6$, $Na_{10}Ge_2P_6$ and $Li_{10}Si_2P_6$,[6,12] all of which exhibit one Wyckoff position for the tetrel element. In $Na_{10}AlTaP_6$, the tetravalent tetrel atom of the latter is substituted by a trivalent aluminum and a pentavalent tantalum atom in a 1:1 ratio on a single mixed atom position. The unit cell volume of the isotypic tetrel compounds at room temperature increases with the size of the alkali metal and of the tetrel element ($Li_{10}Si_2P_6$: $V = 555.7$ Å^3; $Na_{10}Si_2P_6$: 760.9 Å^3; $Na_{10}Ge_2P_6$: 780.3 Å^3), and the volume of $Na_{10}AlTaP_6$ (787.18(4) Å^3) is slightly larger than that of the Na/Ge compound in agreement with the increasing ionic radii (Si^{4+} 0.40 Å, Ge^{4+} 0.53 Å, Al^{3+} 0.53 Å; Ta^{5+} not listed for coordination no. 4),[46–47] as are the M–P bond lengths (mean M–P in $Li_{10}Si_2P_6$: 2.257 Å; $Na_{10}Si_2P_6$: 2.294 Å; $Na_{10}Ge_2P_6$: 2.381 Å; $Na_{10}AlTaP_6$: 2.418 Å).

MAS NMR spectroscopy of $Na_{10}AlTaP_6$. The ^{31}P and ^{23}Na MAS NMR spectra of $Na_{10}AlTaP_6$ are shown in Figure 3. The ^{31}P MAS NMR spectrum contains two broad signals with chemical shifts of 150.19 and −290.04 ppm, accompanied by a sharp signal at -205 ppm which is attributed to a 1.5 % Na_3P[48] impurity (after integration of all signals). Due to its low concentration this impurity was not detected in the powder X-ray diffractogram.

In Figure 3a, the two broad signals are marked with a triangle and a star, respectively, with the filled markers belonging to the isotropic signals and the empty markers to the corresponding rotation side bands as confirmed by two separate measurements at different rotational frequencies (see Figure S8). The integration of the two signals, including all rotation side bands, gives an almost exact integral ratio of 4:2 (150.19 ppm: −290.04 ppm). The broader signal at 150.19 ppm is rather asymmetric, and one might assume a third small signal at roughly 105 ppm.

The chemical shifts of phosphorus atoms in known phosphide compounds are listed in Table 2. As observed in Na_7TaP_4, the resonances of P atoms covalently bonded to Ta atoms are downfield-shifted compared to that of P atoms attached to Si or Al. As in $Li_{10}Si_2P_6$, the bridging P atoms can usually be distinguished from the terminal ones by NMR spectroscopy.[6] Comparing the shift values of $Na_{10}AlTaP_6$ to those of known compounds, the signals at 150.19 and 105 ppm are in the range of P atoms attached to Ta like in Na_7TaP_4,[41] and the signal at −290.04 ppm is in the range of P atoms coordinated to Al like in Li_3AlP_2.[10]

In order to confirm the interpretation of the ^{31}P and ^{23}Na MAS NMR spectra of $Na_{10}AlTaP_6$, we calculated the chemical

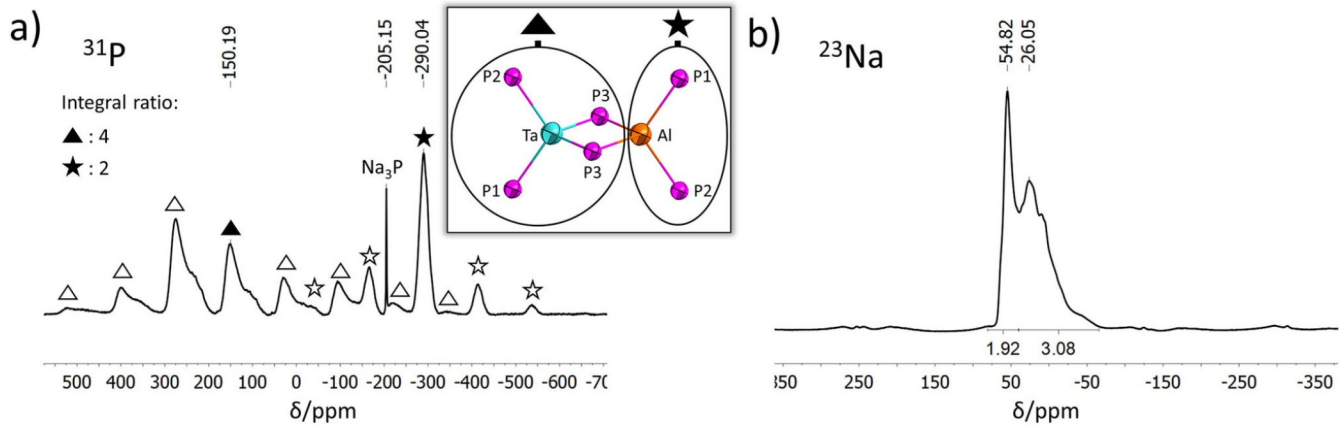

Figure 3. ^{31}P (a) and ^{23}Na (b) MAS NMR spectra of $Na_{10}AlTaP_6$. a) The ^{31}P NMR spectrum shows two signals with an approximate ratio of 4:2 at 150.19 and −290.04 ppm, respectively, which are indicated by triangles and stars. The filled markers belong to the isotropic signals and the corresponding unfilled markers to the rotation side bands. Furthermore, the spectrum shows small amounts of impurities of Na_3P (−205.15 ppm). The ^{23}Na NMR spectrum exhibits two broad signals. These two signals can roughly be assigned in a ratio of 2 (54.82 ppm):3 (26.05 ppm) according to the five different Na Wyckoff positions.

Table 2. Comparison of the chemical shifts of P atoms in $Na_{10}AlTaP_6$, Na_7TaP_4, Li_8SiP_4, Li_2SiP_2, $Li_{10}Si_2P_6$, and Li_3AlP_2.[6–7,10,41]

Compound	Bonding situation of phosphorus	Chemical shifts
$Na_{10}AlTaP_6$	(1b-P^{2-})-Ta	+150.19 ppm
	(2b-P^{-})-Ta/Al	~ +105 ppm
	(1b-P^{2-})-Al	−290.04 ppm
Na_7TaP_4	(1b-P^{2-})-Ta	+113.03 ppm– +53.98 ppm
Li_8SiP_4	(1b-P^{2-})-Si	−225.3 and −251.3 ppm.
Li_2SiP_2	(2b-P^{-})-Si	−129.1 and −241.5
$Li_{10}Si_2P_6$	(2b-P^{-})-Si	−124.1
	(1b-P^{2-})-Si	−188.4 ppm/ −198.5 ppm
Li_3AlP_2	(2b-P^{-})-Al	−300.07 ppm– −308.72 ppm

shifts with the DFT-PBE method on the basis of an ordered structural model with mixed $AlTaP_6$ dimers. The ^{31}P chemical shifts with respect to $(NH_4)H_2PO_4$ are −235 ppm for (1b-P^{2-})-Al, 142 ppm for (1b-P^{2-})-Ta and 166 ppm for (2b-P^{-}). Each chemical shift corresponds to two P atoms, leading to a 4:2 ratio for the positive and negative chemical shifts, in agreement with the experimental findings. The (1b-P^{2-})-Al signal at −235 ppm is underestimated compared to the experimental value of −290.04 ppm, but the result is in line with the underestimated ^{31}P chemical shift for Na_3P (calc. −125 ppm, exp. −205 ppm). A recent systematic benchmark study on ^{31}P NMR chemical shift predictions with DFT methods has showed that the differences between DFT-GGA and experimental ^{31}P NMR chemical shifts are larger for the more upfield-shifted P atoms.[49] A better agreement between the theory and experiment could be achieved with hybrid DFT methods, but they are not yet generally available for solid-state NMR studies.

The ^{23}Na MAS NMR spectrum shows two overlapping signals at a chemical shift of 54.82 and 26.05 ppm, respectively, with a ratio of 2:3. This fits perfectly to the five crystallographic Na Wyckoff positions of equal multiplicity, three of which are octahedrally and two are tetrahedrally coordinated by P atoms. The more downfield-shifted signal at 54.82 ppm is assigned to the tetrahedrally coordinated Na atoms and the more upfield-shifted signal at 26.05 ppm to the octahedrally coordinated Na atoms. This is in good agreement with NMR experiments in silicates, where the octahedrally coordinated Na atoms are upfield-shifted compared to the tetrahedrally coordinated ones.[50]

We also calculated the ^{23}Na chemical shifts with the DFT-PBE method. The average shift value with respect to solid NaCl is 94 ppm (shifts vary between 70–132 ppm). Although the chemical shift is overestimated in comparison to the experimental one, it is in qualitative agreement. A better agreement between theory and experiments could be expected when for example thermal effects are included, which are completely lacking in the current 0 K calculations.

Raman spectroscopy of $Na_{10}AlTaP_6$. The Raman spectrum of powdered $Na_{10}AlTaP_6$ is shown in Figure 4. For the assignment of the most intense mode at 389 cm^{-1}, a theoretical Raman spectrum was calculated at the DFT-PBE0/TZVP level of theory, and the harmonic frequencies of the calculated Raman spectrum were scaled by a factor of 0.955 in order to match the highest intensity modes of the experimental spectrum. As described above, a structural model including an ordered dimer of edge-sharing TaP_4 and AlP_4 tetrahedra was used for the calculation instead of a mixed occupation of Al and Ta at the same position. The experimental and calculated Raman spectra are in very good agreement (Figure 4). The strongest vibrational band at 389 cm^{-1} represents the symmetric stretching of the TaP_4 unit with an additional movement of the Al atom towards the Ta atom. This intense mode is in very good accordance with

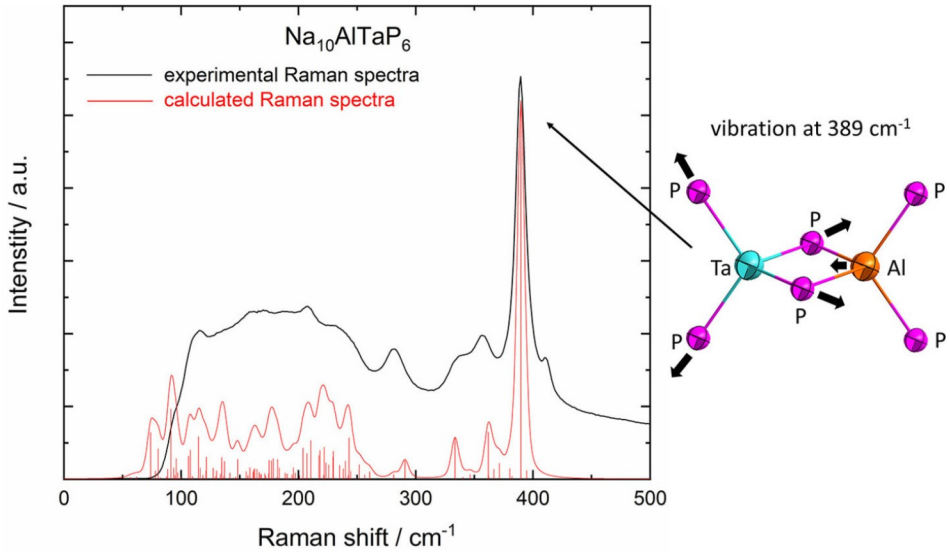

Figure 4. Experimental (black) and calculated (red) Raman spectra for $Na_{10}AlTaP_6$. The wavenumbers of the calculated Raman spectrum have been scaled by a factor of 0.955 in order to match the highest intensity modes of the experimental spectrum. The most intense frequency at 389 cm^{-1} corresponds to the symmetrical stretching mode of the TaP_4 tetrahedra in a $TaAlP_6$ dimer.

that of the symmetrical vibration of the isolated TaP_4 tetrahedra in Na_7TaP_4 at 378 cm^{-1}.[41]

Impedance spectroscopy of $Na_{10}AlTaP_6$. Since several Li-rich ternary phosphides show high Li ion conductivities, impedance measurements were performed to determine the ionic conductivity of $Na_{10}AlTaP_6$ (Figure S9). The semi-circle can be described as parallel circuit element of a resistor and a constant phase element (*R*/*Q*). For the constant phase element the fit of the data acquired at 298 K resulted in α values of ≈ 0.85 and *Q* parameters of $\approx 8\times10^{-8}\,F\cdot s^{(\alpha-1)}$; the conductivity was determined to $\sigma(Na_{10}AlTaP_6) = 1.9(2)\times10^{-7}\,S\,cm^{-1}$ at 298 K (obtained from two independently measured cells). DC polarization measurements in the range from 50 to 150 mV reveal an electronic conductivity of $1.3(2)\times10^{-7}\,S\cdot cm^{-1}$ at 298 K (based on the standard deviation of two cells) (Figure S10). The conductivity value obtained by DC polarization measurements is in the same range as the value received by PEIS measurements. Hence, the Nyquist plot shows only the semi-circle of the electronic conductivity, but no semi-circle for the ionic conductivity. The absence of ion conductivity might be ascribed to structural reasons, since - at least for all so far observed good phosphide-based Li ion conductors - the presence of partially empty octahedral voids within the close-packed P anions seems to be an important requirement for the mobility of Li^+ ions.[1–2,7] The larger Na^+ ions are found preferably in an octahedral coordination of P atoms, and thus all octahedral voids of the close-packed P atoms in $Na_{10}AlTaP_6$ are occupied, and consequently these convenient ion migration paths are blocked, and no significant ion conduction contribution can be detected.

Crystal structure of Na_3GaP_2. Red single crystals of Na_3GaP_2 were obtained from the reaction of the elements in the ratio Na:Ga:P = 9:1:4 at 1073 K in a tantalum tube. Besides Na_3GaP_2, the resulting mixture of products contains Na_6GaP_3, TaP and, according to unassigned diffractions in the powder X-ray diffractogram, at least one unknown phase (see Figure S6). Details of the structure refinement of the single crystal X-ray diffraction of Na_3GaP_2 are listed in Table 1 (further data are given in Tables S6 and S7 in the Supporting Information).

Na_3GaP_2 crystallizes in the orthorhombic space group *Ibam* (no. 72), with four independent crystallographic positions (Na1, Na2, Ga, P). The crystal structure is shown in Figure 5. It is built up by $[GaP_4]$ tetrahedra stacked together via edge-sharing in infinite one-dimensional chains $^1_\infty[GaP_2]^{3-}$ which are surrounded by Na counter ions (Figure 5a and b), and which are isovalence-electronic to the chains in SiS_2.[51] Assuming the usual oxidation states Na^+, Ga^{3+} and P^{3-}, Na_3GaP_2 can be written as the electronically balanced formula $(Na^+)_3[GaP_2]^{3-}$.

As expected from the Ga^{3+}-Ga^{3+} repulsions within the chains the GaP_4 tetrahedra are slightly elongated with one smaller P–Ga–P angle of 100.88(1)° compared to the remaining ones of 113.47(2)° and 114.39(2)°. The Ga–P bonds of 2.4380(3) Å are longer than those observed in compounds with interconnected GaP_4 tetrahedra like in Li_3GaP_2 (2.404–2.419 Å)[10] or in the binary phase GaP (2.3601 Å),[52] and they are shorter than the Ga–P distances observed in Li_9GaP_4 with isolated GaP_4 units (2.4404 and 2.4584 Å).[5] All sodium atoms exhibit strongly distorted coordination environments (see Figure S3). The distortion of the NaP_4 tetrahedra (Na1) is reflected by the P–Na–P angles ranging from 90.33(1)° to 125.29(1)°, and the distortion of the NaP_6 octahedra (Na2) is documented by a wide range of Na–P distances between 2.8422(8) and 4.276(1) Å, indicating also that the Na atoms are not located in the center of gravity of the P_6 octahedra. The lighter homolog Li_3GaP_2 contains infinite two-dimensional layers of edge- and corner-sharing GaP_4 tetrahedra, and thus the substitution of the smaller lithium

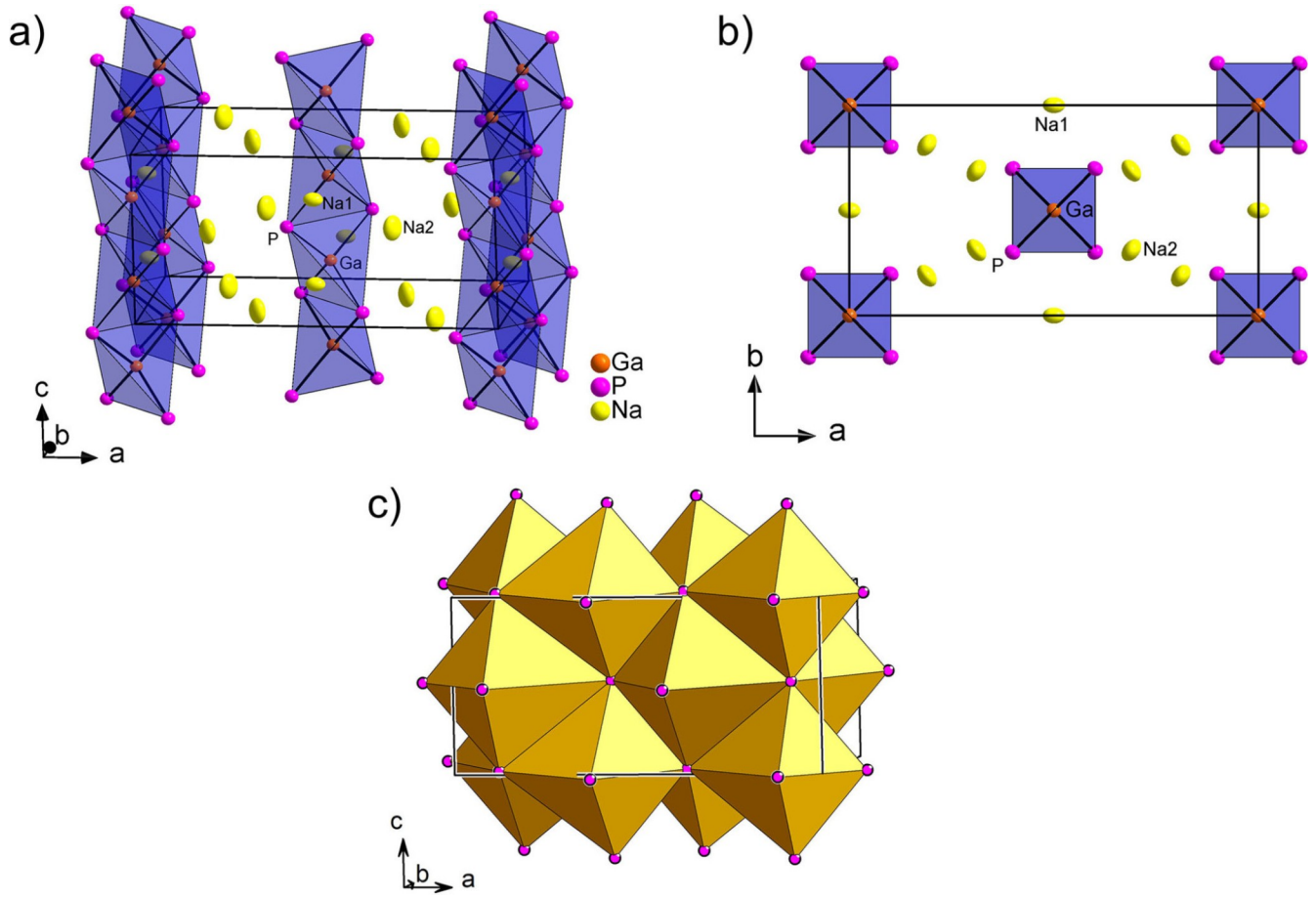

Figure 5. The crystal structure of Na_3GaP_2. a) Extended unit cell. The GaP_4 tetrahedra are arranged in infinite chains of edge-sharing tetrahedra. b) View along [001]. c) Unit cell of Na_3GaP_2 with the edge-sharing NaP_6 octahedra, illustrating the *ccp* of the phosphorous atoms. The Na, Ga and P atoms are drawn in yellow, orange and purple, respectively. The displacement ellipsoids are shown at a 90% probability level at 150 K.

by sodium leads to a segregation of this layer and an arrangement of the resulting edge-sharing GaP_4 tetrahedra in chains.[10]

The crystal structure is built up by a distorted cubic close packing of phosphorus atoms, which is shown in Figure 5, Figure 5c by the presence of exclusively edge sharing NaP_6 octahedra. With respect to the multiplicity of the phosphorous' Wyckoff positions (8*j*), the orthorhombic unit cell contains 16 tetrahedral and 8 octahedral voids. One quarter of the tetrahedral voids is filled by gallium atoms (Wyckoff position 4*a*), and the sodium atoms are located in all octahedral positions (Na2: 8*j*) and in one quarter of the tetrahedral voids (Na1: 4*b*), resulting in a 50% filling of the tetrahedral voids. Na_3GaP_2 is isotypic to the known aluminum homolog Na_3AlP_2,[17,53] and both show the same kind of polyanionic partial structure as the orthorhombic phase Na_2SiP_2, which contains infinite chains of edge-sharing SiP_4 tetrahedra.[13] However, in Na_3GaP_2 and Na_3AlP_2 the chains run parallel to each other, whereas they are rotated against each other in Na_2SiP_2. This results in a more irregular arrangement, reflected by the additional presence of NaP_x trigonal bipyramids and trigonal prisms besides octahedra. As expected, the unit cell volume increases with higher amounts of sodium and with the size of the triel element (ionic radii for CN 4: Al^{3+} 0.53 Å and Ga^{3+} 0.61 Å)[46–47] from Na_2SiP_2 ($V = 1727.43(11)$: $4 = 431.86(3)$ Å^3) over Na_3AlP_2 (540.53(13) Å^3) to Na_3GaP_2 (546.6(2) Å^3).

Electronic structures of $Na_{10}AlTaP_6$ and Na_3GaP_2. The electronic structures were investigated by quantum chemical methods at the DFT-PBE0/TZVP level of theory. The optimized structures are in good agreement with the experimental findings, except for the *b* lattice parameter of Na_3GaP_2, which deviates from the experimental value by 5.8% (Table S9). Band structure calculations show that $Na_{10}AlTaP_6$ and Na_3GaP_2 are both semiconductors with indirect band gaps of 2.9 eV (Figure 6).

In both cases the density of states reveals that Na, Al and Ta, respectively, have almost no contribution to the uppermost valence bands, where P has the highest contribution. In $Na_{10}AlTaP_6$, Ta shows the highest contribution to the conduction band, while Na, Ga and P contribute almost equally to the conduction bands of Na_3GaP_2.

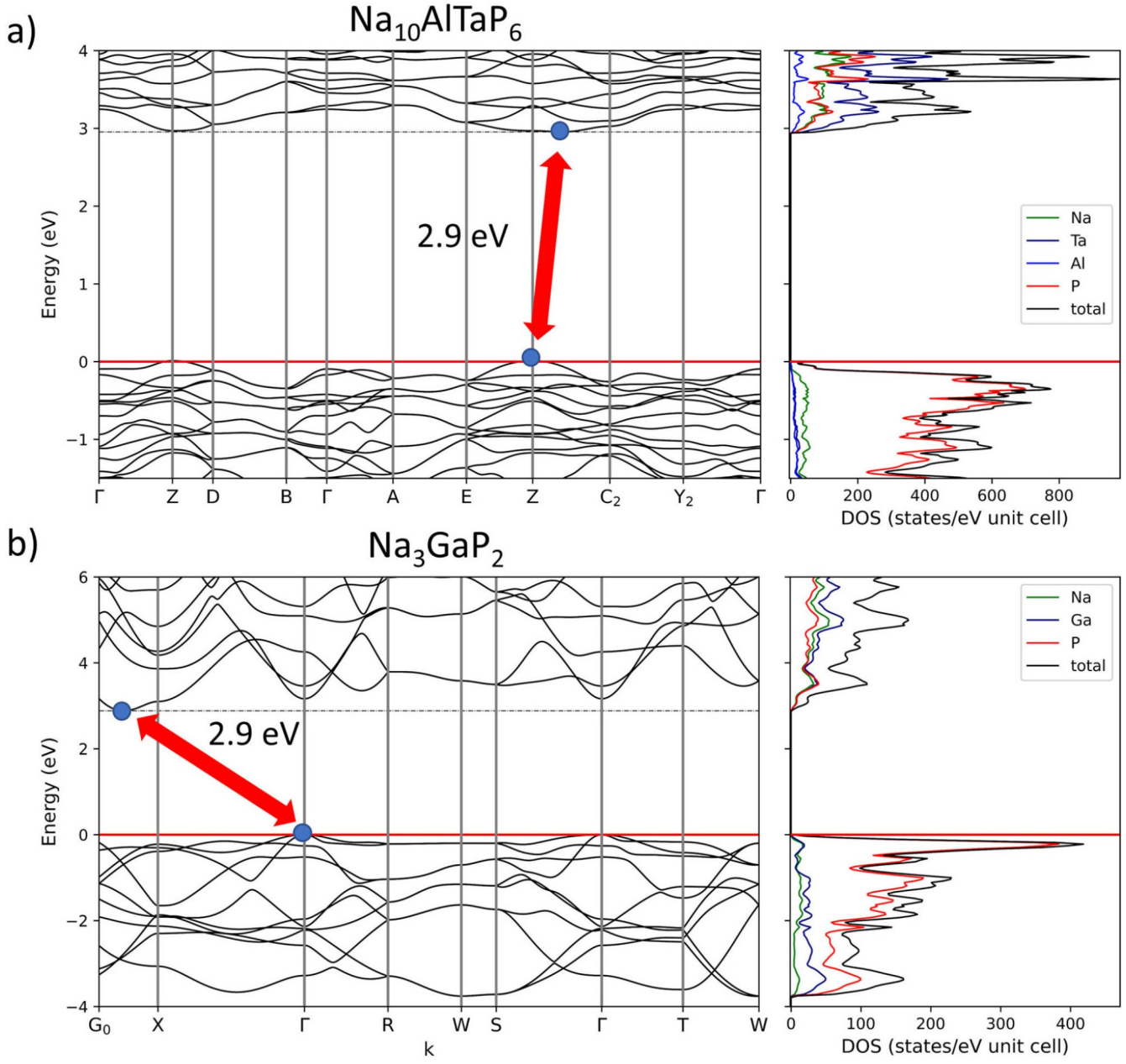

Figure 6. Band structure and density of states (DOS) of $Na_{10}AlTaP_6$ and Na_3GaP_2, both exhibiting indirect bands gap of 2.9 eV. The Fermi level is located at 0 eV.

Conclusions

The two compounds $Na_{10}AlTaP_6$ and Na_3GaP_2 have been synthesized and characterized. Both compounds contain edge-sharing MP_4 tetrahedra, which are usually less favored due to the short distance and, therefore, strong repulsion between the central atoms. Apparently, the presence of the large P^{3-} ions and the resulting long *M*–P bonds overrule this disadvantage, and even in the presence of the highly charged Ta^{5+} an edge-sharing arrangement becomes stable. $Na_{10}AlTaP_6$ with its dimers of $(Al_{0.5}Ta_{0.5})P_4$ tetrahedra is the first example of an aliovalent substitution of a tetravalent tetrel atom by a group 13/15 combination of metal atoms, which indicates a notable intrinsic stability of this structure type. In the sodium phosphidogallate Na_3GaP_2, this motif of edge-sharing MP_4 tetrahedra is even more extended by the formation of infinite, one-dimensional chains. These chains are stable with different elements as central atoms and are formed with different amounts of separating alkali metals, i.e. with different overall chain charges, as they are known from (neutral) SiS_2, from the sodium phosphidosilicate Na_2SiP_2 and from the lighter homolog of the gallate, Na_3AlP_2, the latter even is an isotypic structure.

$Na_{10}AlTaP_6$ shows no ion conductivity. The crystal structure consists of a distorted *hcp* of phosphorous atoms, where half of

the tetrahedral and all octahedral voids are filled by cations. Having in mind that in the related lithium compounds free octahedral voids are essential for a noteworthy ion conduction, this result supports the understanding of the conduction process. The aliovalent substitution of the tetravalent tetrel element by the trivalent aluminum and the pentavalent tantalum opens the possibility to trigger the lithium content and the defect concentration in the ion conducting phases Li_8TtP_4, $Li_{14}TtP_6$ (Tt = Si, Ge, Sn) and Li_9AlP_4 by the aliovalent substitution by tantalum, which will be followed up in our future studies.

Associated Content

Supporting Information

Details of the crystal structure determination, experimental powder X-ray diffraction pattern, coordination polyhedra, electrochemical characterization, details on DFT calculations

Acknowledgements

The work was carried out as part of the research project ASSB coordinated by ZAE Bayern. The project is funded by the Bavarian Ministry of Economic Affairs, Regional Development and Energy. We thank Christoph Wallach for recording the Raman spectrum. Open access funding enabled and organized by Projekt DEAL.

Keywords: phosphide · crystal structure · aluminum · tantalum · gallium

[1] S. Strangmüller, H. Eickhoff, D. Müller, W. Klein, G. Raudaschl-Sieber, H. Kirchhain, C. Sedlmeier, V. Baran, A. Senyshyn, V. L. Deringer, L. van Wüllen, H. A. Gasteiger, T. F. Fässler, *J. Am. Chem. Soc.* **2019**, *141*, 14200–14209.
[2] H. Eickhoff, S. Strangmüller, W. Klein, H. Kirchhain, C. Dietrich, W. G. Zeier, L. van Wüllen, T. F. Fässler, *Chem. Mater.* **2018**, *30*, 6440–6448.
[3] S. Strangmüller, H. Eickhoff, G. Raudaschl-Sieber, H. Kirchhain, C. Sedlmeier, L. van Wüllen, H. A. Gasteiger, T. F. Fässler, *Chem. Mater.* **2020**, *32*, 6925–6934.
[4] T. M. F. Restle, C. Sedlmeier, H. Kirchhain, W. Klein, G. Raudaschl-Sieber, V. L. Deringer, L. v. Wüllen, H. A. Gasteiger, T. F. Fässler, *Angew. Chem. Int. Ed.* **2020**, *59*, 5665–5674; *Angew. Chem.* **2020**, *132*, 5714–5723.
[5] T. M. F. Restle, C. Sedlmeier, H. Kirchhain, W. Klein, G. Raudaschl-Sieber, L. v. Wüllen, T. F. Fässler, *Chem. Mater.* **2021**, *33*, 2957–2966.
[6] H. Eickhoff, L. Toffoletti, W. Klein, G. Raudaschl-Sieber, T. F. Fässler, *Inorg. Chem.* **2017**, *56*, 6688–6694.
[7] L. Toffoletti, H. Kirchhain, J. Landesfeind, W. Klein, L. van Wüllen, H. A. Gasteiger, T. F. Fässler, *Chem. Eur. J.* **2016**, *22*, 17635–17645.
[8] H. Eickhoff, C. Sedlmeier, W. Klein, G. Raudaschl-Sieber, H. A. Gasteiger, T. F. Fässler, *Z. Anorg. Allg. Chem.* **2020**, *646*, 95–102.
[9] A. Haffner, T. Bräuniger, D. Johrendt, *Angew. Chem.* **2016**, *128*, 13783–13786; *Angew. Chem. Int. Ed.* **2016**, *55*, 13585–13588.
[10] T. M. F. Restle, J. V. Dums, G. Raudaschl-Sieber, T. F. Fässler, *Chem. Eur. J.* **2020**, *26*, 6812–6819.
[11] T. M. F. Restle, V. L. Deringer, J. Meyer, G. Raudaschl-Sieber, T. F. Fässler, *Chem. Sci.* **2021**, *12*, 1278.1285.
[12] B. Eisenmann, M. Somer, *Z. Naturforsch.* **1985**, *40b*, 886–890.
[13] A. Haffner, A.-K. Hatz, C. Hoch, B. V. Lotsch, D. Johrendt, *Eur. J. Inorg. Chem.* **2020**, *2020*, 617–621.
[14] K. Feng, W. Yin, R. He, Z. Lin, S. Jin, J. Yao, P. Fu, Y. Wu, *Dalton Trans.* **2012**, *41*, 484–489.
[15] H. Eickhoff, Dissertation, Technische Universität München, **2019**.
[16] A. Haffner, A.-K. Hatz, I. Moudrakovski, B. V. Lotsch, D. Johrendt, *Angew. Chem. Int. Ed.* **2018**, *57*, 6155–6160; *Angew. Chem.* **2018**, *130*, 6263–6268.
[17] M. Somer, W. Carrillo-Cabrera, E. M. Peters, H. G. v. Schnering, *Z. Kristallogr.* **1995**, *210*, 777–777.
[18] W. Blase, G. Cordier, M. Somer, *Z. Kristallogr.* **1991**, *195*, 119–120.
[19] W. Blase, G. Cordier, M. Somer, *Z. Kristallogr.* **1993**, *206*, 143–144.
[20] *WinXPOW*, 3.0.2.1, STOE & Cie GmbH, Darmstadt, Germany, **2011**.
[21] *TOPAS*, 6, Bruker AXS, **2016**.
[22] G. Sheldrick, *Acta Crystallogr. Sect. C: Struct. Chem.* **2015**, *71*, 3–8.
[23] *WiRe 4.2*, Renishaw plc, Gloucestershire, **2002**.
[24] R. Dovesi, A. Erba, R. Orlando, C. M. Zicovich-Wilson, B. Civalleri, L. Maschio, M. Rerat, S. Casassa, J. Baima, S. Salustro, B. Kirtman, *WIREs Comput. Mol. Sci.* **2018**, *8*, e1360.
[25] J. P. Perdew, K. Burke, M. Ernzerhof, *Phys. Rev. Lett.* **1996**, *77*, 3865–3868.
[26] C. Adamo, V. Barone, *J. Chem. Phys.* **1999**, *110*, 6158–6170.
[27] F. Weigend, M. Häser, H. Patzelt, R. Ahlrichs, *Chem. Phys. Lett.* **1998**, *294*, 143–152.
[28] F. Weigend, R. Ahlrichs, *Phys. Chem. Chem. Phys.* **2005**, *7*, 3297–3305.
[29] H. J. Monkhorst, J. D. Pack, *Phys. Rev. B* **1976**, *13*, 5188–5192.
[30] F. Pascale, C. M. Zicovich-Wilson, F. L. Gejo, B. Civalleri, R. Orlando, R. Dovesi, *J. Comput. Chem.* **2004**, *25*, 888–897.
[31] C. M. Zicovich-Wilson, F. Pascale, C. Roetti, V. R. Saunders, R. Orlando, R. Dovesi, *J. Comput. Chem.* **2004**, *25*, 1873–1881.
[32] L. Maschio, B. Kirtman, M. Rérat, R. Orlando, R. Dovesi, *J. Chem. Phys.* **2013**, *139*, 164101.
[33] L. Maschio, B. Kirtman, M. Rérat, R. Orlando, R. Dovesi, *J. Chem. Phys.* **2013**, *139*, 164102.
[34] T. J. Team, Jmol – An Open-Source Java Viewer for Chemical Structures in 3D. *http://www.jmol.org/*, The Jmol Team, **2019**.
[35] Y. Hinuma, G. Pizzi, Y. Kumagai, F. Oba, I. Tanaka, *Comput. Mater. Sci.* **2017**, *128*, 140–184.
[36] A. Hjorth Larsen, J. Jørgen Mortensen, J. Blomqvist, I. E. Castelli, R. Christensen, M. Dułak, J. Friis, M. N. Groves, B. Hammer, C. Hargus, E. D. Hermes, P. C. Jennings, P. Bjerre Jensen, J. Kermode, J. R. Kitchin, E. Leonhard Kolsbjerg, J. Kubal, K. Kaasbjerg, S. Lysgaard, J. Bergmann Maronsson, T. Maxson, T. Olsen, L. Pastewka, A. Peterson, C. Rostgaard, J. Schiøtz, O. Schütt, M. Strange, K. S. Thygesen, T. Vegge, L. Vilhelmsen, M. Walter, Z. Zeng, K. W. Jacobsen, *J. Phys. Condens. Matter* **2017**, *29*, 273002.
[37] S. J. Clark, M. D. Segall, C. J. Pickard, P. J. Hasnip, M. J. Probert, K. Refson, M. C. Payne, *Z. Kristallogr.* **2005**, *220*, 567–570.
[38] C. J. Pickard, F. Mauri, *Phys. Rev. B* **2001**, *63*, 245101.
[39] J. R. Yates, C. J. Pickard, F. Mauri, *Phys. Rev. B* **2007**, *76*, 024401.
[40] D. Vanderbilt, *Phys. Rev. B* **1990**, *41*, 7892–7895.

[41] T. M. F. Restle, J. V. Dums, G. Raudaschl-Sieber, W. Klein, T. F. Fässler, *Inorg. Chem.* **2020**, *59*, 18420–18426.
[42] J. Lin, W. Hönle, H. G. von Schnering, *J. Alloys Compd.* **1992**, *183*, 403–412.
[43] J. Nuss, H. Kalpen, W. Hönle, M. Hartweg, H. G. von Schnering, *Z. Anorg. Allg. Chem.* **1997**, *623*, 205–211.
[44] M. Lulei, W. Carrillo-Cabrera, H. G. v. Schnering, *Z. Kristallogr. New Cryst. Struct.* **1998**, *213*, 485–485.
[45] H. Eickhoff, C. Dietrich, W. Klein, W. G. Zeier, T. F. Fässler, *Z. Anorg. Allg. Chem.* **2021**, *647*, 28–33.
[46] R. D. Shannon, C. T. Prewitt, *Acta Crystallogr. Sect. B* **1969**, *25*, 925–946.
[47] R. D. Shannon, *Acta Crystallogr. Sect. A* **1976**, *32*, 751–767.
[48] L. E. Marbella, M. L. Evans, M. F. Groh, J. Nelson, K. J. Griffith, A. J. Morris, C. P. Grey, *J. Am. Chem. Soc.* **2018**, *140*, 7994–8004.
[49] P. Gao, J. Zhang, H. Chen, *Int. J. Quantum Chem.* **2021**, *121*, e26482.
[50] X. Xue, J. F. Stebbins, *Phys. Chem. Miner.* **1993**, *20*, 297–307.
[51] W. Büssem, H. Fischer, E. Gruner, *Naturwissenschaften* **1935**, *23*, 740–740.
[52] A. Addamiano, *J. Am. Chem. Soc.* **1960**, *82*, 1537–1540.
[53] L. Ohse, M. Somer, W. Blase, G. Cordier, *Z. Naturforsch. B* **1993**, *48*, 1027–1034.

Manuscript received: April 24, 2021
Revised manuscript received: May 27, 2021
Accepted manuscript online: June 2, 2021

